

RESEARCH ARTICLE

HIV-1 THERAPY

Sustained virologic control in SIV⁺ macaques after antiretroviral and $\alpha_4\beta_7$ antibody therapy

Siddappa N. Byrareddy,^{1*} James Arthos,^{2*} Claudia Cicala,^{2*} Francois Villinger,^{1,3,†} Kristina T. Ortiz,¹ Dawn Little,¹ Neil Sidell,⁴ Maureen A. Kane,⁵ Jianshi Yu,⁵ Jace W. Jones,⁵ Philip J. Santangelo,⁶ Chiara Zurlo,⁶ Lyle R. McKinnon,^{7,§} Kelly B. Arnold,⁸ Caroline E. Woody,⁸ Lutz Walter,⁹ Christian Roos,⁹ Angela Noll,⁹ Donald Van Ryk,² Katija Jelacic,² Raffaello Cimbrotto,¹⁰ Sanjeev Gumber,³ Michelle D. Reid,¹ Volkan Adsay,¹ Praveen K. Amancha,³ Ann E. Mayne,¹ Tristram G. Parslow,¹ Anthony S. Fauci,² Aftab A. Ansari^{1||}

Antiretroviral drug therapy (ART) effectively suppresses replication of both the immunodeficiency viruses, human (HIV) and simian (SIV); however, virus rebounds soon after ART is withdrawn. SIV-infected monkeys were treated with a 90-day course of ART initiated at 5 weeks post infection followed at 9 weeks post infection by infusions of a primatized monoclonal antibody against the $\alpha_4\beta_7$ integrin administered every 3 weeks until week 32. These animals subsequently maintained low to undetectable viral loads and normal CD4⁺ T cell counts in plasma and gastrointestinal tissues for more than 9 months, even after all treatment was withdrawn. This combination therapy allows macaques to effectively control viremia and reconstitute their immune systems without a need for further therapy.

Profound and durable suppression of HIV by antiretroviral therapy (ART) represents a major accomplishment in HIV-AIDS research. However, HIV persists in patients despite long-term ART therapy such that, once ART is withdrawn, virus invariably rebounds. Lifetime ART treatment is associated with toxicity (1), residual chronic inflammation, and the accelerated onset of diseases associated with aging (2, 3).

High levels of viral replication in gastrointestinal tissues (GITs) during acute infection lead to severe depletion of local CD4⁺ T cells (4), damage to the gut epithelium, and the rapid formation of persistent viral reservoirs. Generalized immune dysfunction and chronic immune activation follow. Even when administered days after infection, ART fails to fully reverse these insults (5). We reasoned that preventing HIV-susceptible cells from accessing GITs might reduce damage to the gut and the mucosal immune system in a way that would allow immune mechanisms to effectively control infection.

A principal pathway that CD4⁺ T cells use to traffic into GITs involves an interaction between integrin $\alpha_4\beta_7$, expressed on CD4⁺ T cells, with mucosal vascular addressin cell adhesion molecule 1 (MAdCAM-1), expressed primarily on high endothelial venules within GITs (6, 7). CD4⁺ T cells that express high levels of the $\alpha_4\beta_7$ integrin ($\alpha_4\beta_7^{\text{hi}}$) are preferential targets of HIV and simian immunodeficiency virus (SIV) during acute infection (8–12). In order to disrupt trafficking of $\alpha_4\beta_7^{\text{hi}}$ CD4⁺ T cells into GITs, we developed a recombinant rhesus monoclonal antibody against the heterodimeric form of $\alpha_4\beta_7$ ($\alpha_4\beta_7$ mAb) that blocks $\alpha_4\beta_7$ binding to MAdCAM (13–15).

Administration of $\alpha_4\beta_7$ mAb before and during repeated low-dose intravaginal SIV challenge of rhesus macaques (RMs) leads to significant protection from transmission (13). In treated animals that became infected, GIT CD4⁺ T cells were preserved and GIT proviral DNA was reduced,

and thus, virus-mediated damage to GITs was minimized.

Because ART provides only partial protection to GITs (5, 14), we considered the possibility that adding $\alpha_4\beta_7$ mAb might improve this protection. To this end, we conducted a study in genetically characterized (table S1, A to D) SIV-infected RMs that combined a 90-day course of ART, beginning 5 weeks post-infection with a series of eight infusions of $\alpha_4\beta_7$ mAb. This treatment strategy included five phases as outlined in fig. S1. In phase I (weeks 1 to 5), 18 RMs were infected intravenously with a 200 median tissue culture infectious dose (TCID₅₀) of SIVmac239. After 5 weeks, all 18 animals began a 90-day daily regimen of ART (phase II). During phase III (weeks 9 to 18), 11 animals received $\alpha_4\beta_7$ mAb once every 3 weeks (eight infusions total); 7 animals received nonspecific rhesus immunoglobulin G (IgG). During phase IV (weeks 18 to 32), ART was withdrawn, and $\alpha_4\beta_7$ mAb–IgG treatment was continued. In phase V (weeks 32 to 50), all treatment was terminated. Three out of 11 $\alpha_4\beta_7$ mAb-treated animals developed antibodies against the $\alpha_4\beta_7$ mAb (fig. S2) and were excluded from further analysis.

ART + $\alpha_4\beta_7$ mAb controls plasma and gut viral loads

All 15 animals showed similar peaks in viremia around weeks 2 to 3 ($\sim 2.9 \times 10^6$ copies/ml), and they all fully suppressed viremia by 3 weeks after ART initiation. The two groups developed divergent viral load (VL) patterns after ART was withdrawn (phase IV). In all seven IgG-treated animals, viremia rebounded to high levels ($\sim 10^6$ copies/ml) within 2 weeks and maintained those levels out to week 50 (Fig. 1B). In contrast, two out of eight $\alpha_4\beta_7$ mAb-treated animals never rebounded, and the remaining six out of eight rebounded but then regained control of viremia within 4 weeks (Fig. 1A). Virologic control was robust in all eight $\alpha_4\beta_7$ mAb-treated animals, with either complete control or transient low-level blips of viremia. The difference in viremia between the two groups after discontinuation of ART was significant ($P < 0.0001$) (Fig. 1C). Virologic control in all eight $\alpha_4\beta_7$ mAb-treated animals persisted to week 81 (fig. S3), although the last infusion of $\alpha_4\beta_7$ mAb (half-life of ~ 11.4 days) was administered at week 32 (13).

Both treatment groups showed similar levels of proviral DNA in GITs during phases I and II. Immediately after cessation of ART, all monkeys showed increases in proviral DNA. High levels (20 to 40 copies/ng DNA) persisted in the seven IgG-treated animals until week 50 (Fig. 1E). In contrast, in all eight $\alpha_4\beta_7$ mAb-treated macaques, proviral DNA decreased to levels at or below the level of detection by week 30 (Fig. 1D). The difference in the geometric means of the two groups (Fig. 1F) during phases IV and V was significant ($P < 0.0001$). Undetectable proviral DNA loads in all eight $\alpha_4\beta_7$ mAb-treated macaques persisted well after the final infusion of $\alpha_4\beta_7$ mAb (week 32). Thus, combining $\alpha_4\beta_7$ mAb therapy with short-term ART promoted persistent systemic and

¹Department of Pathology and Laboratory Medicine, Emory University School of Medicine, Atlanta, GA 30322, USA.

²Laboratory of Immunoregulation, NIAID, NIH, Bethesda, MD 20892, USA. ³Division of Pathology, The Yerkes National Primate Center of Emory University, Atlanta, GA 30329, USA.

⁴Department of Obstetrics and Gynecology, Emory University School of Medicine, Atlanta, GA 30322, USA. ⁵Department of Pharmaceutical Sciences, School of Pharmacy, University of Maryland, Baltimore, MD 21201, USA. ⁶Wallace H. Coulter Department of Biomedical Engineering, Georgia Institute of Technology and Emory University, Atlanta, GA 30680, USA.

⁷Centre for the AIDS Program of Research in South Africa (CAPRISA), Durban, South Africa. ⁸Department of Biomedical Engineering, University of Michigan, Ann Arbor, MI 48109, USA. ⁹Primate Genetics Laboratory, German Primate Center, Leibniz Institute for Primate Research, Göttingen, Germany.

¹⁰Division of Rheumatology, Johns Hopkins School of Medicine, Baltimore, MD 21201, USA.

*These authors contributed equally to the planning and performance of this study. †Present address: Department of Pharmacology and Experimental Neuroscience, University of Nebraska Medical Center, Omaha, NE 68198, USA. ‡Present address: Office of the Director, New Iberia Research Center, University of Louisiana at Lafayette, New Iberia, LA 70560, USA. §Present address: Department of Medical Microbiology, University of Manitoba, Winnipeg, Canada. ||Corresponding author. Email: pathaa@emory.edu

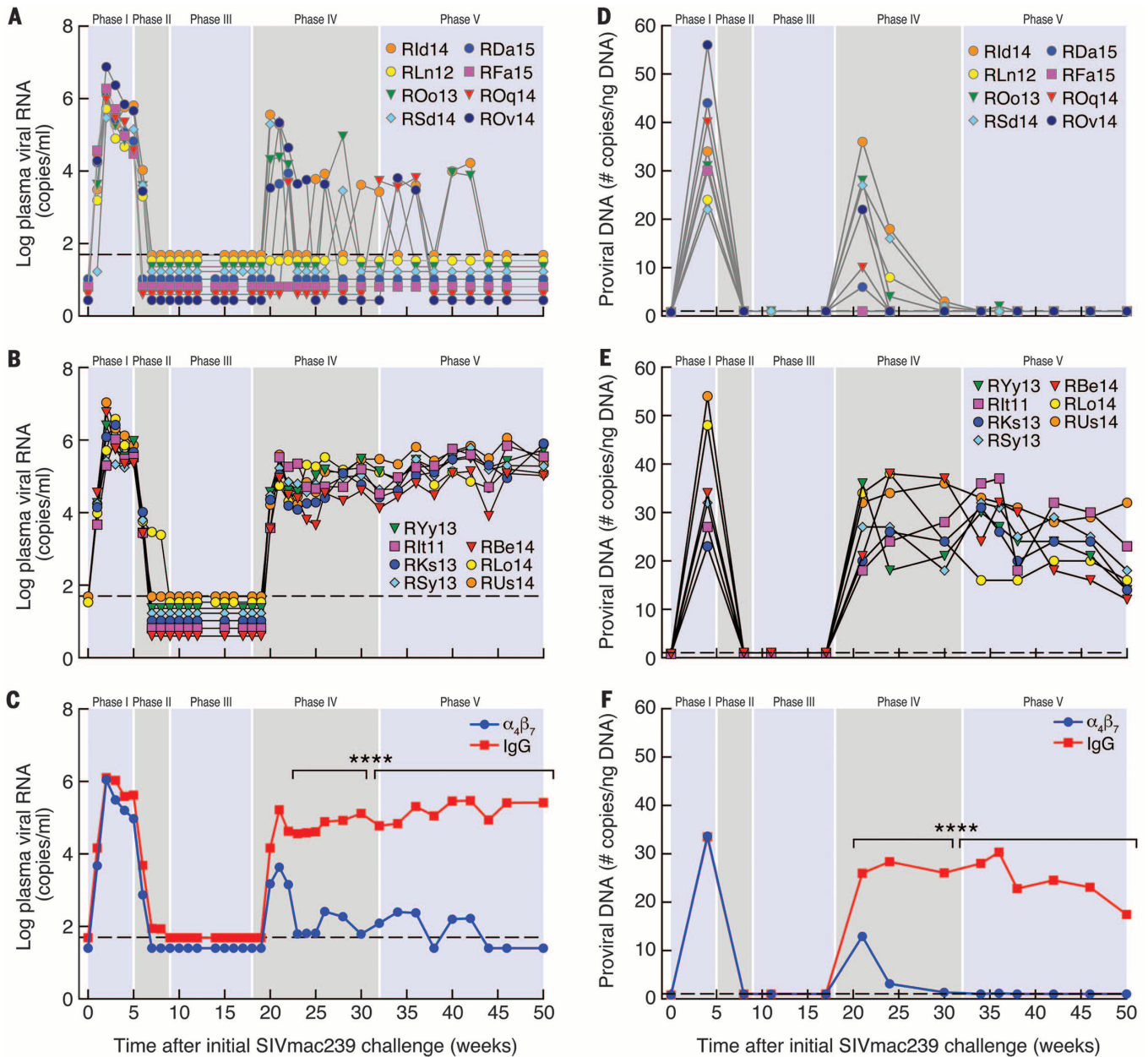


Fig. 1. Control of plasma and GIT viral loads. Plasma viral loads from (A) eight monkeys receiving ART + $\alpha_4\beta_7$ mAb and (B) seven monkeys receiving ART + IgG are reported as log₁₀ number of viral copies/ml of plasma. (C) Geometric means for plasma viral loads of monkeys treated with ART + $\alpha_4\beta_7$ mAb (blue) or IgG (red). GIT proviral DNA loads for (D) eight monkeys receiving ART + $\alpha_4\beta_7$ mAb and (E) seven monkeys receiving IgG are

reported as the number of copies of proviral DNA/ng of total DNA. (F) Geometric means for GIT proviral loads of monkeys treated with ART + $\alpha_4\beta_7$ mAb (blue) or IgG (red). The shaded areas in each graph demarcate the five phases of the study. Code names of individual monkeys are shown in each graph. *P* values were determined using analysis of covariance (ANCOVA) (*****P* < 0.0001).

mucosal virologic control following discontinuation of all therapy.

Rebound of CD4⁺ T cell subsets

Blood and GIT mononuclear cells isolated from each phase of the study were analyzed by flow cytometry (table S2, A to C). During phase I, the absolute numbers of blood total CD4⁺ T cells and subsets showed a sharp decline (Fig. 2, A to D). After the first administration of $\alpha_4\beta_7$ mAb (phase III), CD4 values diverged. The $\alpha_4\beta_7$ mAb-treated

animals, but not controls, showed marked increases in total CD4⁺ T cells and, notably, in the effector memory (EM) CD4⁺ T cell subset (>four-fold increase, *P* < 0.0001) (Fig. 2D). These increases were sustained after discontinuation of the $\alpha_4\beta_7$ mAb treatment (phase V). By week 50, total CD4⁺ T cell numbers approached preinfection levels.

Acute HIV-1 and SIV infections are characterized by a rapid depletion of CD4⁺ T cells in GITs (4, 15–18). Therefore, we evaluated the fate of GIT CD4⁺ T cells (Fig. 2, E to H), with values expressed

as the percent of CD4⁺ T cells within the gated population of CD45⁺ cells. We observed a sharp decline in total CD4⁺ T cells during the acute phase in both groups with CD45⁺/CD4⁺ T cells reaching their nadir by the end of phase I (Fig. 2E). In phase III, the CD4⁺ T cell profile of the two treatment groups diverged. The relative frequency of CD45⁺/CD4⁺ cells in the $\alpha_4\beta_7$ mAb-treated animals gradually increased through phase V (*P* < 0.0001). CD4⁺ T cell subsets showed an apparent recovery of both T central memory (CM)

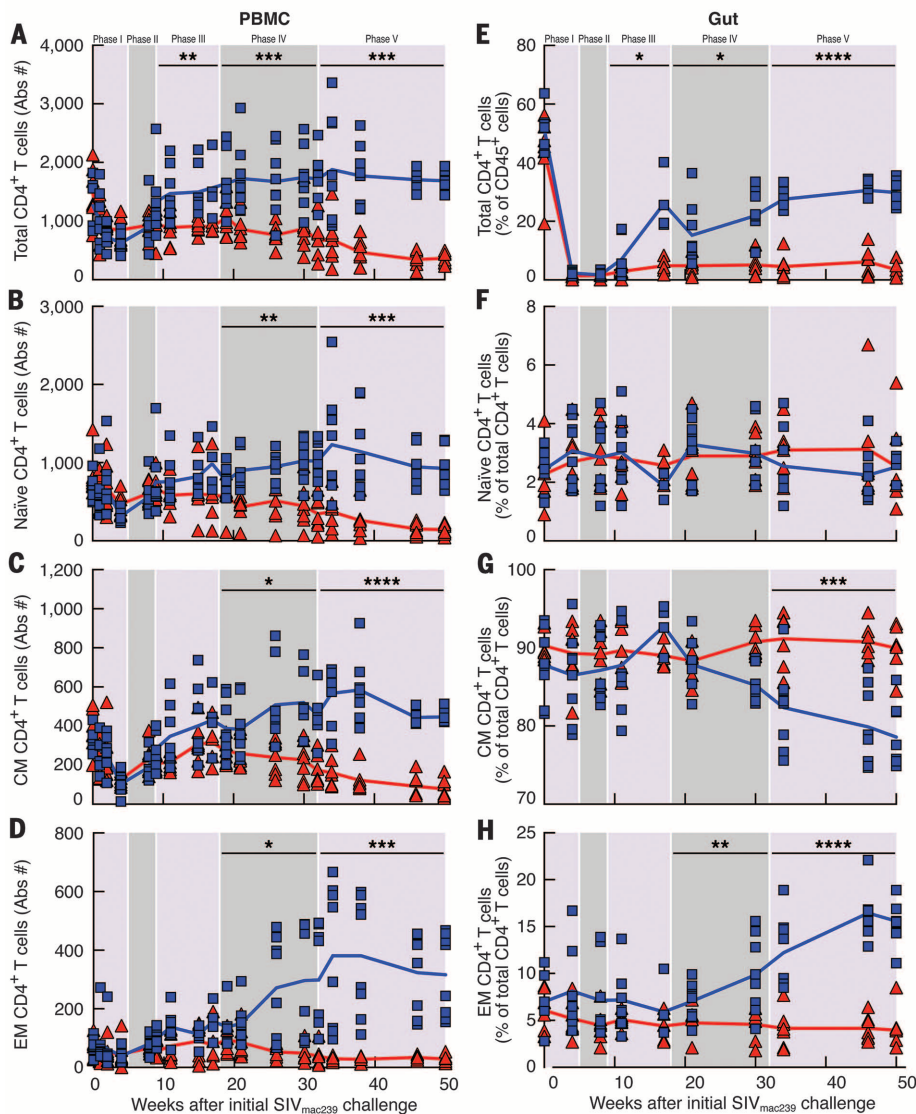


Fig. 2. Kinetic changes in CD4⁺ T cell subsets. Kinetic changes in the absolute number of circulating CD4⁺ T cells in (A) PBMCs and subsets, (B) naïve CD4⁺ T cells, (C) T central memory (T_{CM}) CD4⁺ T cells, and (D) T effector memory (T_{EM}) CD4⁺ T cells. $\alpha_4\beta_7$ mAb-treated monkeys (blue) and IgG-treated animals (red). Frequencies in GITs of (E) total CD4⁺ T cells expressed as the percentage of the gated population of CD45⁺ cells, (F) naïve CD4⁺ T cells, (G) T_{CM} CD4⁺ T cells, and (H) T_{EM} CD4⁺ T cells. The frequencies of CD4⁺ T cell subsets in GITs were calculated as the percentage of total CD4⁺ T cells in the same sample. *P* values were determined using the multiple *t* test (**P* < 0.05; ***P* < 0.01; ****P* < 0.001; *****P* < 0.0001).

and T EM cells in the $\alpha_4\beta_7$ mAb-treated animals, with the EM recovering at a faster rate (Fig. 2, G and H). The relative proportion of naïve CD4⁺ T cells remained constant through phase V (Fig. 2F). The quality of this recovery was well reflected by increases in the frequencies of T helper 17 (T_H17) and T helper 22 (T_H22) subsets of CD4⁺ T cells in both GITs and blood (fig. S4) (19). Consistent with these results, immunohistological analysis of GIT sections after week 50 revealed abundant CD4⁺ T cells in $\alpha_4\beta_7$ mAb-treated animals but not in controls (fig. S5).

To better understand the repopulation of gut tissues with CD4⁺ T cells, we used a newly developed antibody-targeted positron emission tomog-

raphy (immuno-PET) combined with the computed tomography (CT) imaging technique (20). Around week 50 (phase V), four macaques from each treatment group were imaged with a ⁶⁴Cu-labeled F(ab')₂ antibody against CD4. Although we had originally hypothesized that $\alpha_4\beta_7$ mAb would inhibit CD4⁺ T cell trafficking to GITs, we instead observed repopulation of CD4⁺ cells in a wide variety of immune tissues, including GITs (Fig. 3). This result suggests that the protective effect of $\alpha_4\beta_7$ mAb in minimizing GIT viral load early in infection (Fig. 1, D to F) facilitated the repopulation of CD4⁺ cells throughout the systemic and mucosal immune systems. It is unclear whether the reconstitution of these immune sites resulted from the control of vi-

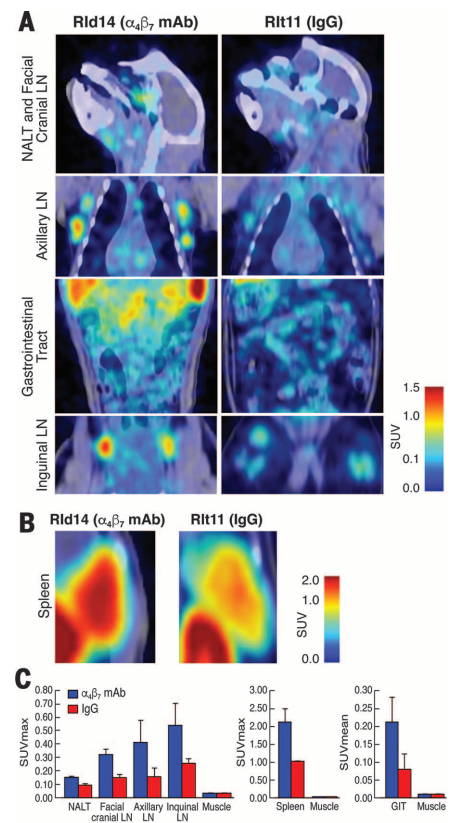


Fig. 3. Immuno-PET-CT analysis confirms the preservation of CD4⁺ cells. PET-CT image analysis of four IgG- and four $\alpha_4\beta_7$ mAb-treated monkeys with ⁶⁴Cu-labeled anti-CD4 F(ab')₂ mAb around week 50 post infection. (A) Representative images of the nasal-associated lymphoid tissues (NALTs), facial cranial lymph nodes (LN), axillary LN, GI tract, and inguinal LN from a monkey receiving $\alpha_4\beta_7$ mAb (Rld14) (left) and a monkey receiving IgG (Rlt11) (right). (B) Images of spleen from $\alpha_4\beta_7$ mAb-treated (Rld14) (left) and IgG-treated (Rlt11) (right). (C) Average (means \pm SD) signals obtained from four $\alpha_4\beta_7$ mAb-treated and four IgG-treated animals for NALTs, facial cranial LN, axillary LN, inguinal LN, GITs, and muscle. Values shown are SUVmax [density of highest signal obtained within a region of interest (ROI)] for all tissues except GITs, where SUVmean is reported (mean of signals within an ROI).

remia, whether these immune competent components contributed to virologic control, or both.

Phenotypic analysis of NK cells and other cell lineages

Total natural killer (NK) cells in blood remained similar in both groups during phases I to IV (Fig. 4) and decreased during phase V but only in the IgG-treated group (Fig. 4A). We observed a decrease in the cytolytic subset (NKG2a⁺/CD8⁺/CD16⁺/CD56⁻) during phase III and IV in the $\alpha_4\beta_7$ mAb-treated group, followed by an increase during phase V (Fig. 4B). Cytokine-synthesizing NK cells (NKG2a⁺/CD8⁺/CD16⁺/CD56⁺) increased during phase IV in $\alpha_4\beta_7$ mAb-treated animals

(Fig. 4C). By week 50, these values approached baseline. A related pattern was observed in GITs. In the $\alpha_4\beta_7$ mAb-treated group, the proportion of the cytokine-synthesizing NK cell subset increased through phases IV and V (Fig. 4H), with corresponding decreases in the proportion of other NK cell subsets. These changes are noteworthy in two ways. First, among all NK cell subsets analyzed, $\alpha_4\beta_7$ expression is highest (~40%) on cytokine-synthesizing NK cells. Second, these increases coincided with the appearance of virologic control in phase IV. Frequencies of NKG2A⁺ CD8⁺ CD16⁺ CD56⁺ innate lymphoid cells (ILCs) decreased in both treatment groups as early as phase I (fig. S6), which is consistent with the loss of ILCs in acute HIV infection (21). However, we observed a sustained increase in the frequency of ILCs in gut biopsies in ART + $\alpha_4\beta_7$ mAb-treated animals beginning in phase III but not in controls. Note that vaccine-induced ILCs have been correlated with protection from SIV infection (22). Other cell lineages (CD8⁺ T cells, B cells, and plasmacytoid and myeloid dendritic cells) were analyzed (figs. S7 and S8), as were activation markers on CD4⁺, CD8⁺ T and NK cells (figs. S9 to S11). Although differences were noted, further studies will be required to inform the impact of those differences.

Identification of signature plasma cytokines

Results presented above suggest that virologic control was immune mediated. To this end, we analyzed a panel of 20 immune or inflammatory markers (table S3) in plasma samples. To identify signatures for each of the five phases of the study, we used a partial least square discriminant analysis (PLSDA). PLSDA models were created for the five study phases by using measurements from each sample and time point, and variable importance projection scores were used to omit markers that did not contribute to group differentiation. Cross-validation was used to assess model performance. In phases I and II, we found no distinction between treatment groups, with a high cross-validation error between models (0.28 and 0.21, respectively) (fig. S12, A and B). In phases III to V, distinct signatures differentiated the two treatment groups, with low cross-validation errors in each phase (0.09, 0.02, and 0, respectively) (Fig. 5A). The differentiating signature varied in each of these phases. One common feature of all three was a comparative increase in retinoic acid (RA) in the $\alpha_4\beta_7$ mAb-treatment group (Fig. 5B). The signature in phase III, when both groups were aviremic, included increases in interleukin-21 (IL-21), granulocyte-macrophage colony-stimulating factor, soluble CD14 (sCD14), interferon- α (IFN- α), as well as RA; however, IFN- γ and transforming growth factor- β (TGF- β) were reduced. In phases IV and V, $\alpha_4\beta_7$ mAb treatment was associated with increased IL-10 and RA, with comparative decreases of proinflammatory markers, including IL-1 β , IFN- γ -induced protein (IP-10), complement-reactive protein (CRP), the coagulation biomarker D-dimer, and two markers, sCD163 and intestinal

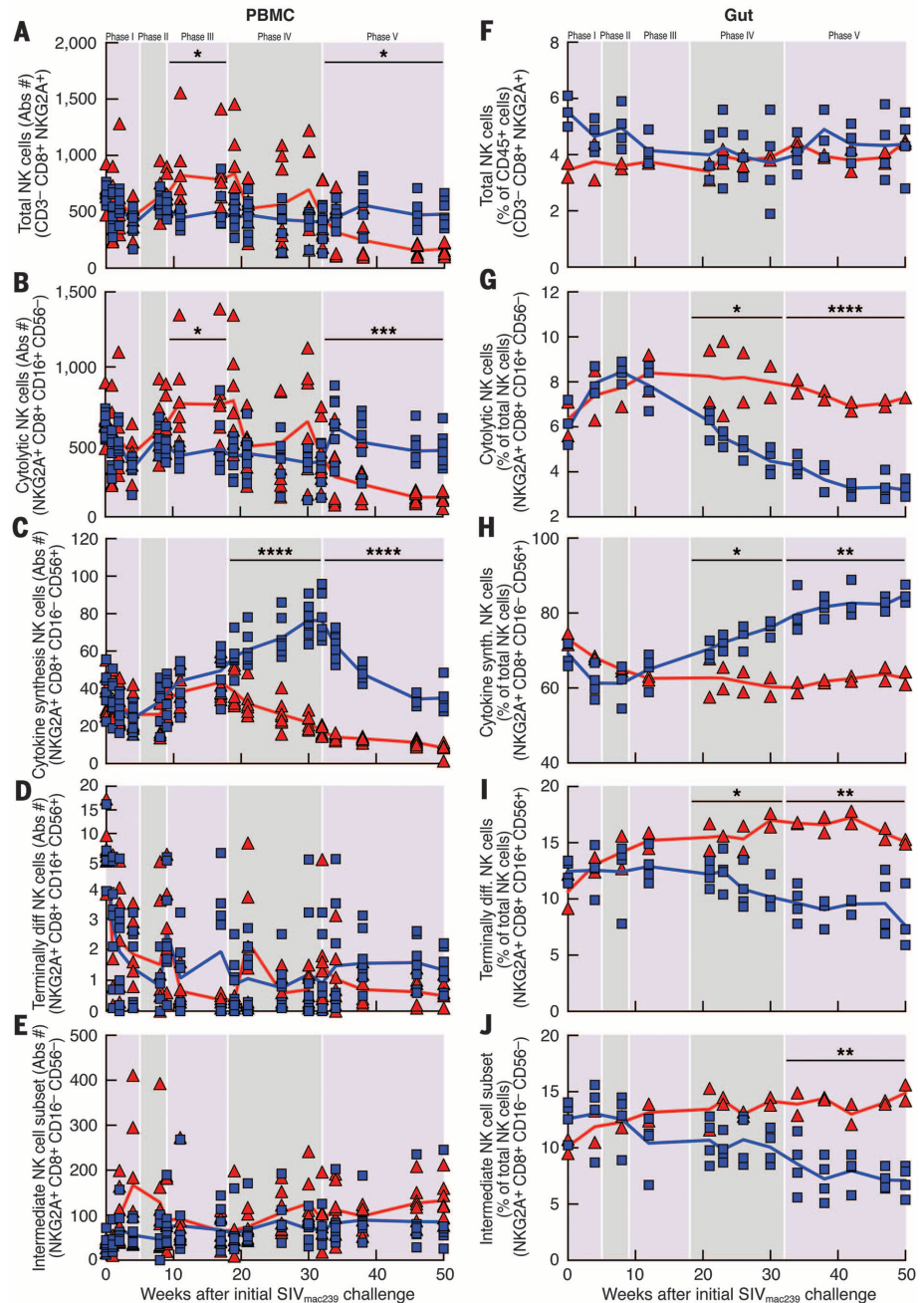


Fig. 4. Kinetic changes in the frequencies of NK cell subsets. The absolute numbers of circulating (A) total NK cells in PBMCs, (B) cytolytic NK cells, (C) cytokine-synthesizing NK cells, (D) terminally differentiated NK cells, and (E) intermediate NK cells. Monkeys treated with ART + $\alpha_4\beta_7$ mAb (blue) and the ART + rhesus IgG (red). Frequencies in GITs of (F) total NK cells as a percentage of CD45⁺ cells, (G) cytolytic NK cells, (H) cytokine synthesizing NK cells, (I) terminally differentiated NK cells, and (J) intermediate NK cells. The frequencies of NK cell subsets in GITs were calculated as the percentage of total NK cells in the same sample. *P* values were determined using the multiple *t* test (**P* < 0.05; ***P* < 0.01; ****P* < 0.001; *****P* < 0.0001).

fatty acid-binding protein (I-FABP), associated with gut permeability (Fig. 5A and fig. S13).

ART + $\alpha_4\beta_7$ mAb restores plasma retinoic acid levels

RA induces the expression of $\alpha_4\beta_7$ (23, 24) and also plays an essential role in gut homeostasis

(23, 25–27). Baseline RA levels decreased during acute infection in both groups (Fig. 5B). A similar response was observed in two uninfected monkeys afflicted with chronic diarrhea (fig. S14), suggesting that such declines are linked to gut inflammation. Of note, measurements taken on weeks 15, 17, and 19 (phase III) differentiated

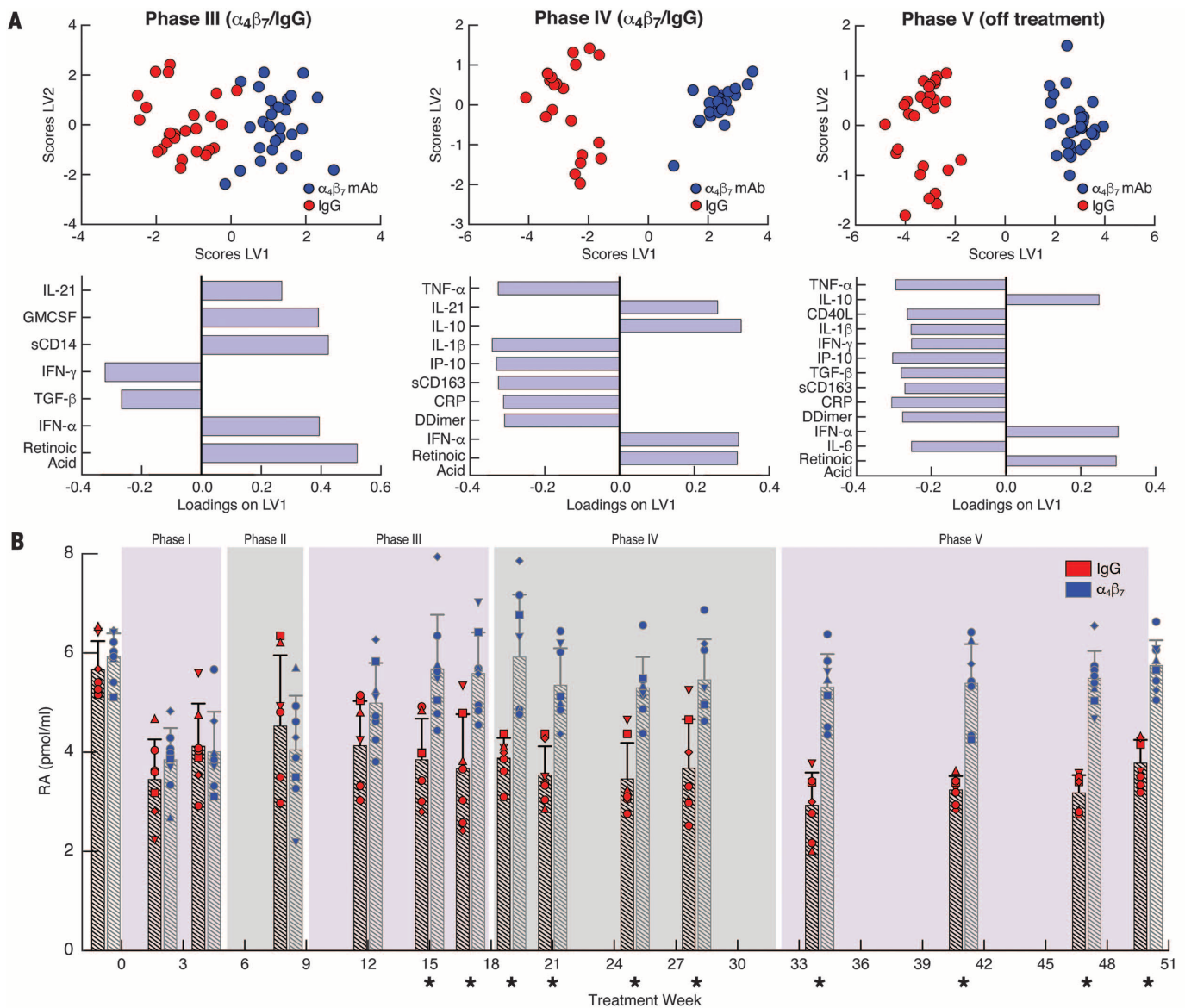


Fig. 5. Multivariate cytokine signatures and plasma levels of retinoic acid. (A) Separate PLSDA models for phases III (left), IV (middle), and V (right). Score plots of latent variable 1 (LV1) versus LV2 (top). Monkeys treated with $\alpha_4\beta_7$ mAb (blue) and IgG (red). Corresponding loadings plots (bottom) with the multivariate cytokine signatures for each phase. (B) Plasma levels (means \pm SD) of RA are displayed (pmol/ml) in the individual monkeys treated with $\alpha_4\beta_7$ mAb (blue) and IgG (red) through all five phases of the study (denotes unpaired *t* test, **P* < 0.003).

the two groups, such that RA in the $\alpha_4\beta_7$ treatment group recovered to near-baseline levels. To understand whether these changes reflected the administration of $\alpha_4\beta_7$ mAb, independent of SIV infection, we treated two uninfected animals with $\alpha_4\beta_7$ mAb and observed no effect on serum RA (fig. S15). Indeed, we also observed a similar response in I-FABP levels in phase III (fig. S13). Finally, we carried out an exploratory analysis to identify additional biomarkers in phase III that might correlate with the degree of gut proviral DNA rebound in phase IV. Both positive and negative predictors of the magnitude of viral rebound in gut tissues were identified (fig. S16).

Induction of gp120 V2-specific antibody responses

Plasma and peripheral blood mononuclear cell (PBMC) samples were also screened for SIV-specific antibody responses and antibody-dependent cell-mediated cytotoxicity (ADCC). We found neither neutralizing antibodies nor differences in ADCC titers (fig. S17). In human and macaque vaccine trials, nonneutralizing antibodies directed against the second variable loop (V2) in Env glycoprotein 120 (gp120) correlated with reduced risk of acquisition (28, 29). We therefore characterized the specificity of the antibody responses by performing Pepscan enzyme-linked immunosorbent assay (ELISA) of sera from five animals in each

group against linear peptides spanning the entire gp120 subunit (fig. S18). Serum samples from weeks 30 to 36 showed that five out of five $\alpha_4\beta_7$ mAb-treated macaques reacted, to varying levels, with two overlapping V2 peptides (peptides 26 and 27). None of the IgG-treated controls reacted to both of these peptides (two animals reacted to one peptide). We found no other consistent difference in epitope-specific reactivity between the two groups. We then evaluated antibody responses using a more sensitive surface plasmon resonance (SPR) assay. Sera from all 15 animals through the five treatment phases were reacted with both SIV gp120 and an SIV cyclic V2 peptide. Sera from both treatment

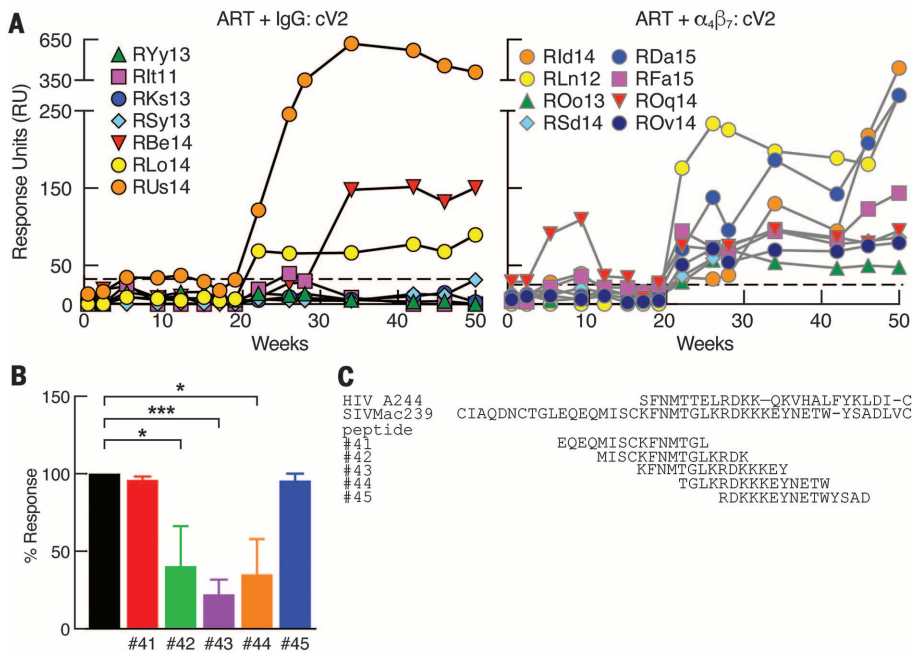


Fig. 6. Characterization of the anti-SIV gp120 V2 antibody response. (A) Reactivity (response units, RU) of sera from individual animals in the groups treated with ART + IgG (top left) and ART + $\alpha_4\beta_7$ mAb (top right) against a cyclic V2 peptide (cV2). The dashed line represents the cut-off value for positive reactivity. (B) Serum reactivity (percent response, means \pm SD) against cV2 of four ART + $\alpha_4\beta_7$ mAb-treated animals in the presence of overlapping V2 peptides (41 to 45), or in the absence of any competing peptide (black bar), defined as 100% response. Asterisk (*) represents the level of significance (* P < 0.05; *** P < 0.001, paired t test for each condition, compared with the no-peptide control). (C) Alignment of the SIV V2 overlapping peptides 41 to 45 with the V2 region of SIVmac239 and the corresponding region of HIV A244 gp120. Single-letter abbreviations for the amino acid residues are as follows: A, Ala; C, Cys; D, Asp; E, Glu; F, Phe; G, Gly; H, His; I, Ile; K, Lys; L, Leu; M, Met; N, Asn; P, Pro; Q, Gln; R, Arg; S, Ser; T, Thr; V, Val; W, Trp; and Y, Tyr. * P < 0.001.

groups showed similar reactivity to gp120 (mean values) (fig. S19). However, the two treatment groups differed in their reactivity to V2. Whereas eight out of eight $\alpha_4\beta_7$ mAb-treated animals showed persistent reactivity to V2, only three out of seven IgG-treated animals reacted to V2 (Fig. 6A). We then fine-mapped this reactivity by competing serum reactivity from all eight animals with overlapping 15mer peptides spanning V2 (Fig. 6B). A peptide corresponding to the sequence KFNMTGLKRDKKKEY (see Fig. 6 legend) reduced serum reactivity by ~80%. Alignment of this sequence with an HIV Thai clade A/E V2 sequence indicates that it recognizes the same region identified in a sieving analysis for immune correlates of reduced risk in the RV144 vaccine trial (Fig. 6C) (30). These data indicate that $\alpha_4\beta_7$ mAb treatment promotes V2 antibody responses by an undefined mechanism.

Discussion

Combining ART with $\alpha_4\beta_7$ mAb promoted prolonged virologic control (Fig. 1 and fig. S3) and the restoration of CD4⁺ T cells. Control persisted long after $\alpha_4\beta_7$ mAb treatment was terminated. It was not associated with neutralizing antibody or classical cell-mediated immune responses (figs. S20 to S24) but instead with reduced damage to GITs. The precise mechanism(s) by which ART +

$\alpha_4\beta_7$ mAb therapy promoted virologic control remains to be defined. However, we identified a series of correlates that individually or in combination may have contributed to that control. These include the recovery of T_H17 and T_H22 subsets of CD4⁺ T cells, significant increases in cytokine-synthesizing NK cells and NKp44⁺ ILCs, skewing of the antibody response toward the gp120 V2 domain, distinguishing plasma biomarkers in phase III followed by signatures associated with reduced gut damage and inflammation in phases IV and V, and the recovery of RA levels. RA is a key regulator of gut immune responses (31, 32) but it also inhibits fibrosis (33).

Vedolizumab, the humanized analog of $\alpha_4\beta_7$ mAb is believed to reduce trafficking of $\alpha_4\beta_7$ -expressing CD4⁺ T cells to GITs. This is the basis for its use in the treatment of inflammatory bowel disease (IBD) (34). Yet, paradoxically, in this study $\alpha_4\beta_7$ mAb promoted the repopulation of GITs with CD4⁺ T cells. Future studies are needed to address the phenotype and functionality of these cells. Such information may help us better understand both the virologic control we are observing and the mechanism of action of drugs like vedolizumab. Vedolizumab belongs to a class of therapeutic agents that are currently in various stages of development for the treatment of IBD (34, 35). It may be possible

to use these drugs as adjunctive agents in the treatment of HIV infection.

REFERENCES AND NOTES

- J. Saison, L. Cotte, C. Chidiac, T. Ferry, *BMJ Case Rep.* 2012 (mar08 1), bcr1020114905 (2012).
- A. H. Warriner, G. A. Burkholder, E. T. Overton, *Infect. Dis. Clin. North Am.* 28, 457–476 (2014).
- L. Barrett, K. R. Fowke, M. D. Grant, *AIDS Rev.* 14, 159–167 (2012).
- R. S. Veazey *et al.*, *Science* 280, 427–431 (1998).
- J. Ananworanich, K. Dubé, N. Chomont, *Curr. Opin. HIV AIDS* 10, 18–28 (2015).
- M. Briskin *et al.*, *Am. J. Pathol.* 151, 97–110 (1997).
- D. J. Erle *et al.*, *J. Immunol.* 153, 517–528 (1994).
- M. Kader *et al.*, *Mucosal Immunol.* 2, 439–449 (2009).
- X. Wang *et al.*, *Mucosal Immunol.* 2, 518–526 (2009).
- C. Cicala *et al.*, *Proc. Natl. Acad. Sci. U.S.A.* 106, 20877–20882 (2009).
- X. Lu *et al.*, *Cell. Mol. Immunol.* 10.1038/cmi.2015.60 (2015).
- E. Martinelli *et al.*, *J. Acquir. Immune Defic. Syndr.* 64, 325–331 (2013).
- S. N. Byrreddy *et al.*, *Nat. Med.* 20, 1397–1400 (2014).
- M. Guadalupe *et al.*, *J. Virol.* 77, 11708–11717 (2003).
- J. M. Brenchley, D. C. Douek, *Mucosal Immunol.* 1, 23–30 (2008).
- Q. Li *et al.*, *Nature* 434, 1148–1152 (2005).
- J. J. Mattapallil *et al.*, *Nature* 434, 1093–1097 (2005).
- S. Mehandru *et al.*, *J. Virol.* 81, 599–612 (2007).
- H. Xu, X. Wang, R. S. Veazey, *J. AIDS Clin. Res.* 5, 302 (2014).
- P. J. Santangelo *et al.*, *Nat. Methods* 12, 427–432 (2015).
- H. N. Kløverpris *et al.*, *Immunity* 44, 391–405 (2016).
- M. Vaccari *et al.*, *Nat. Med.* 22, 762–770 (2016).
- M. Iwata *et al.*, *Immunity* 21, 527–538 (2004).
- A. C. Ross, *Am. J. Clin. Nutr.* 96, 1166S–1172S (2012).
- W. Agace, *Immunol. Lett.* 128, 21–23 (2010).
- S. Sirisinha, *Asian Pac. J. Allergy Immunol.* 33, 71–89 (2015).
- R. Zeng *et al.*, *Mucosal Immunol.* 6, 847–856 (2013).
- R. Gottardo *et al.*, *PLOS ONE* 8, e75665 (2013).
- P. Pegu *et al.*, *J. Virol.* 87, 1708–1719 (2013).
- M. Rolland *et al.*, *Nature* 490, 417–420 (2012).
- Y. Guo, C. Brown, C. Ortiz, R. J. Noelle, *Physiol. Rev.* 95, 125–148 (2015).
- J. A. Hall, J. R. Grainger, S. P. Spencer, Y. Belkaid, *Immunity* 35, 13–22 (2011).
- R. Xiao *et al.*, *J. Dermatol.* 38, 345–353 (2011).
- M. Jovani, S. Danese, *Curr. Drug Targets* 14, 1433–1443 (2013).
- Vedolizumab, FDA Advisory Committee Recommends Approval of Vedolizumab (Drugs.com, 2013); www.drugs.com/nda/vedolizumab_131209.html.

ACKNOWLEDGMENTS

The authors are deeply grateful to the veterinary staff of the Yerkes National Primate Center, particularly S. Ehmert, C. Souder, and the staff of the Research Services. We thank K. Reimann for making the primatized mAbs for our studies. We also thank M. Rao and K. Peachman for the SIV reagents used for the antibody characterization studies, K. Rogers for Fc γ and TRIM5 α sequencing, R. Gelezunias and D. Hazuda for providing the antiretroviral drugs, and A. Weddle and J. Weddle for preparation of all graphics. The data presented in this manuscript are tabulated in the main paper and in the supplementary materials. J.A., C.C., and A.S.F. are inventors on patent no. 20160075786 held by the National Institute of Allergy and Infectious Diseases (NIAID), NIH, that covers the use of antagonists of the interaction between HIV gp120 and $\alpha_4\beta_7$ integrin. The work performed herein was supported by NIAID-NIH R01 AI098628, R01 AI111907, R01 HD077260, U.S. Food and Drug Administration U01FD005266, the Intramural Program of the NIAID, NIH, Bethesda, MD, and the base grant to the Yerkes National Primate Research Center of Emory University NIH-ORIP-OD-510D-11132. Additional support was provided by the University of Maryland School of Pharmacy Mass Spectrometry Center (SOP1841-1QB2014). J.A., C.C., and A.S.F. are inventors in the patent and patent application 20160075786 submitted by the NIAID. The authors declare no competing financial interest.

SUPPLEMENTARY MATERIALS

www.sciencemag.org/content/354/6309/197/suppl/DC1
 Materials and Methods
 Supplementary Text
 Figs. S1 to S24
 Tables S1 to S3
 References (36–51)

12 May 2016; accepted 9 September 2016
 10.1126/science.aag1276

EXTENDED PDF FORMAT
SPONSORED BY



Sustained virologic control in SIV⁺ macaques after antiretroviral and $\alpha_4\beta_7$ antibody therapy

Siddappa N. Byrareddy, James Arthos, Claudia Cicala, Francois Villinger, Kristina T. Ortiz, Dawn Little, Neil Sidell, Maureen A. Kane, Jianshi Yu, Jace W. Jones, Philip J. Santangelo, Chiara Zurla, Lyle R. McKinnon, Kelly B. Arnold, Caroline E. Woody, Lutz Walter, Christian Roos, Angela Noll, Donald Van Ryk, Katija Jelacic, Raffaello Cimbri, Sanjeev Gumber, Michelle D. Reid, Volkan Adsay, Praveen K. Amancha, Ann E. Mayne, Tristram G. Parslow, Anthony S. Fauci and Aftab A. Ansari (October 13, 2016) *Science* **354** (6309), 197-202. [doi: 10.1126/science.aag1276]

Editor's Summary

Antibodies sustain viral control

For many infected individuals, antiretroviral therapy (ART) means that an HIV-1 diagnosis is no longer a death sentence. But the virus persists in treated individuals, and complying with the intense drug regimen to keep virus loads down can be challenging for patients. Seeking an alternative, Byrareddy *et al.* treated ART-suppressed monkeys with antibodies targeting $\alpha_4\beta_7$ integrin. When ART was halted in the antibody-treated animals, viral loads stayed undetectable, and normal CD4 T cell counts were maintained for over 9 months—and persisted—even after stopping the antibody therapy.

Science, this issue p. 197

This copy is for your personal, non-commercial use only.

Article Tools Visit the online version of this article to access the personalization and article tools:

<http://science.sciencemag.org/content/354/6309/197>

Permissions Obtain information about reproducing this article:

<http://www.sciencemag.org/about/permissions.dtl>

Science (print ISSN 0036-8075; online ISSN 1095-9203) is published weekly, except the last week in December, by the American Association for the Advancement of Science, 1200 New York Avenue NW, Washington, DC 20005. Copyright 2016 by the American Association for the Advancement of Science; all rights reserved. The title *Science* is a registered trademark of AAAS.